Chinese Chemical Letters 34 (2023) 107646

Contents lists available at ScienceDirect

Chinese Chemical Letters

journal homepage: www.elsevier.com/locate/cclet

Rationally designed *meso*-benzimidazole-pyronin with emission wavelength beyond 700 nm enabling *in vivo* visualization of acute-liver-injury-induced peroxynitrite

Minghao Ren[a], Chengyong Zhou[a], Linfang Wang[a,*], Xin Lv[b,*], Wei Guo[b]

[a] *Department of Chemistry, Changzhi University, Changzhi 046011, China*
[b] *School of Chemistry and Chemical Engineering, Shanxi University, Taiyuan 030006, China*

ARTICLE INFO

Article history:
Received 29 March 2022
Revised 24 June 2022
Accepted 27 June 2022
Available online 30 June 2022

Keywords:
Near infrared fluorescent dyes
Lysosome-targetable
Fluorescence probe
Peroxynitrite
Acute liver injury

ABSTRACT

Fluorescent dyes with fluorescence emission above 700 nm are favorable for bio-imaging due to the higher tissue transparency and lower background fluorescence. In this study, we present a *meso*-benzimidazole-pyronin platform (SiBMs) with fluorescence emission maxima above 700 nm, which possess good cell permeability, photostability, and lysosomal localization. The great photophysical properties of the SiBMs encouraged us to further exploit their application toward bio-imaging. We synthesized the reduced 'dihydro' derivative HSiBM3 for sensing $ONOO^-$, with high selectivity and sensitivity and a fast fluorescence "off-on" response (within 2 s). Then, we confirmed the potential of HSiBM3 for visualizing exogenous and endogenous $ONOO^-$ in cells and mice. More importantly, HSiBM3 was successfully employed for visualizing acute-liver-injury-induced peroxynitrite.

Near infrared region (NIR) (650−900 nm) fluorescent dyes play an irreplaceable role in fluorescence imaging techniques due to their deep penetration, minimum background fluorescence, and minimum photodamage to test samples, tissues, and animals [1–5]. By replacing the bridging oxygen atom with a $SiMe_2$ group, Si-pyronin dyes show an emission maximum around 660 nm, with a 90-nm red-shift in excitation and emission wavelengths compared with their corresponding pyronine [6–10]. In addition to their emission wavelength being in the NIR, Si-pyronins also maintain excellent photophysical properties, such as considerable fluorescence quantum yields, high molar extinction coefficients, as well as great photostability [11–13]. More importantly, the above-mentioned excellent spectral properties combined with good water solubility, cell permeability, and low cytotoxicity make Si-pyronins highly attractive and prevalent for developing fluorescent probes [14–18] and characteristic fluorophores for labeling or super-resolution imaging [19–25].

Nonetheless, it is still important for researchers to extend the fluorescence emission of Si-pyronin above 700 nm, which is more favorable for imaging due to the higher tissue transparency and lower background fluorescence [26]. Some researchers, such as Nagano and co-workers, modify Si-pyronin by expanding the ring to obtain longer-wavelength dyes (>700 nm) [7]. Guo's and Wang's group synthesized SO_2Rs (emission maximum around 740 nm) and PRs (emission maximum around 710 nm) by replacing the $SiMe_2$ group with a sulfone group and a phosphorus atom, respectively [27,28]. Some researchers synthesized a Si-pyronine with a maximum emission wavelength of approximately 730 nm by introducing an electron-withdrawing phenylethynyl group at the C9 position [29].

As far as we know, introducing CF_3 or CN to the C9 position of pyronin dyes could increase the emission wavelength dramatically [30–32]. Thus, we replaced CN and CF_3 with a benzimidazole group, which not only acted as an electron-withdrawing group but also could be easily modified *via* the nitrogen atom of the benzimidazole 1 position. In this work, we present a *meso*-benzimidazole-pyronin platform (SiBMs) with fluorescence emission maxima above 700 nm by introducing an electron-withdrawing benzimidazole unit at the *meso* position (Scheme 1). SiBMs not only maintain the outstanding spectral properties of the rhodamine family but also perform well in fluorescence imaging, with good cell permeability, photostability, and lysosomal localization. Based on this platform, we synthesized the 'dihydro' derivative HSiBM3 to serve as a perfect NIR fluorescence probe, which could specifically react with peroxynitrite ($ONOO^-$) to produce SiBM3 quickly (within 2 s) and sensitively (with detection limits of 13.5 nmol/L). Then, we determined the applicability of HSiBM3 for visualizing exogenous and endogenous $ONOO^-$ in cells and mice. More importantly, HSiBM3

* Corresponding authors.
E-mail addresses: wanglf1023@163.com (L. Wang), lvxin@sxu.edu.cn (X. Lv).

https://doi.org/10.1016/j.cclet.2022.06.069
1001-8417/

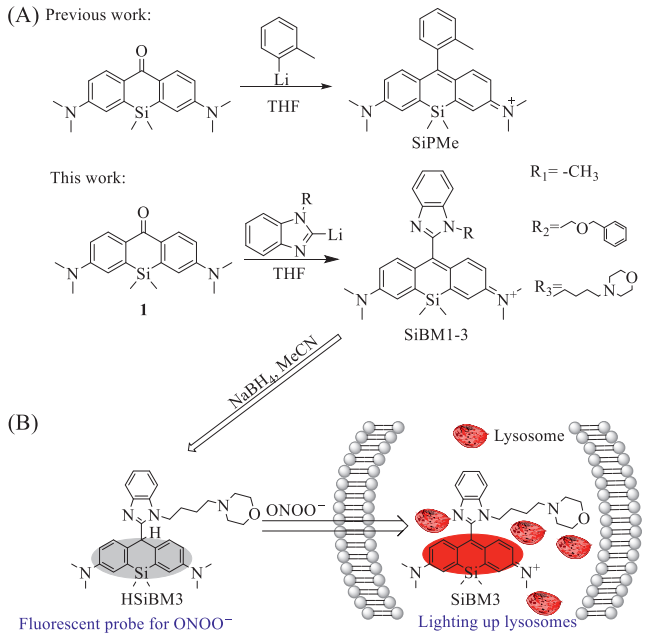

Scheme 1. (A) Synthesis routes of SiPMe and SiBM1-3. (B) Proposed reaction mechanism of HSiBM3 for $ONOO^-$.

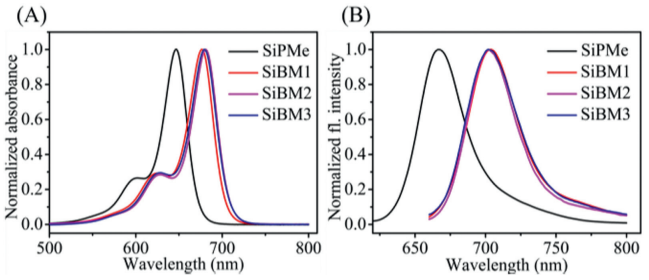

Fig. 1. Normalized absorption (A) and fluorescence (B) spectra of SiBM1-3 (5 μmol/L) and SiPMe (5 μmol/L) in PBS (10 mmol/L, pH 7.4) at 25 °C.

was successfully employed for visualizing peroxynitrite induced by acute liver injury.

As shown in Scheme 1, compound **1** was synthesized by the existing method and then added dropwise to a solution of freshly prepared *N*-methyl benzimidazole-lithiation to give the product SiBM1. Next, we synthesized SiBM2 and SiBM3 by replacing the methyl with a long alkyl chain group. Subsequently, using $NaBH_4$, we synthesized the reductive of HSiBMs to detect reactive oxygen species (ROS). The detailed synthesis steps and data of the above compounds, such as ^1H NMR, ^{13}C NMR, and HRMS spectroscopy, are supplied in Supporting information.

With SiBM1-3 in hand, we first tested their absorption and emission spectra. The absorption and emission spectra in PBS (10 mmol/L, pH 7.4), EtOH, and DCM are illustrated in Fig. 1, Figs. S1 and S2 (Supporting information), respectively. As anticipated, the absorption and emission maxima of SiBM1-3 in PBS (10 mmol/L, pH 7.4) were approximately 680 and 700 nm, respectively, showing a red-shift of 40 nm compared to SiPMe [33]. The absorption and emission maxima were approximative in those different solvents. The photophysical properties of SiBM1-3, such as molar extinction coefficient, Stokes shift, and fluorescence quantum yield, are summarized in Table 1. It was shown that these dyes displayed a considerably high molar extinction coefficient in PBS (10 mmol/L, pH 7.4) solutions, EtOH, and DCM. Moreover, the fluorescence quantum yield of SiBM1 was 0.297 in PBS, 0.184 in EtOH, and 0.12 in

Table 1
Photophysical properties of SiBM1-3 and SiPMe in representative solvents.

Dyes	Solvent	λ_{abs} (nm)	λ_{ex} (nm)	Stoke shift	ε_{max} (L mol^{-1} cm^{-1})	Φ_f
SiBM1	PBS[c]	677	702	25	119400	0.297[b]
	EtOH	680	706	26	125400	0.184[b]
	DCM	679	709	30	137000	0.12[b]
SiBM2	PBS[c]	681	702	21	145100	0.389[b]
	EtOH	682	705	23	151600	0.488[b]
	DCM	681	704	23	161800	0.263[b]
SiBM3	PBS[c]	680	702	22	111400	0.385[b]
	EtOH	682	705	23	111600	0.497[b]
	DCM	680	707	27	118600	0.355[b]
SiPMe	PBS[c]	646	665	29	108400	0.31[a]

[a] Φ_f is the relative fluorescence quantum yield estimated by using cresyl violet as a standard;
[b] Φ_f is the relative fluorescence quantum yield estimated by using Cy5.5 as a standard; $\Phi_f = 0.23$ in water;
[c] PBS (10 mmol/L, containing 0.25% MeCN, pH 7.4).

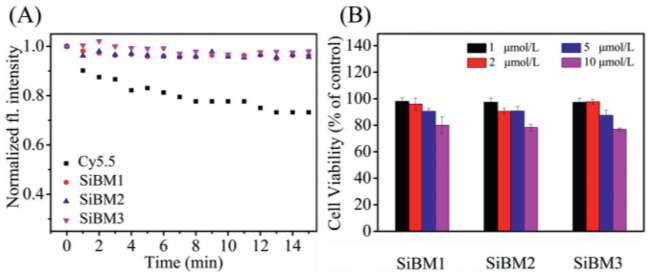

Fig. 2. (A) Normalized time-dependent fluorescence intensity of SiBM1-3 and Cy5.5 continuously irradiated by a Xe lamp for 15 min. (B) Viability of HeLa cells after treating with 1, 2, 5, and 10 μmol/L SiBM1-3 for 24 h.

DCM. SiBM2 and SiBM3 exhibited higher quantum yields (above 0.38 in PBS and 0.48 in EtOH) due to the long aliphatic chains, which can suppress the rotation of the C-C bond. In addition, the good linear relationship (greater than 0.99) between absorption intensity and concentration of SiBMs indicated that SiBM1-3 possessed good water solubility (Fig. S3 in Supporting information).

Subsequently, we studied the stability of SiBM1-3, including pH stability, chemical stability, and photostability. As shown in Fig. S4 (Supporting information), the fluorescence intensity of SiBM1-3 was high at the range of pH 5-10, indicating their suitability for applications under physiological conditions. The absorption maximum of SiBM1-3 at 680 nm decreased and a new absorption maximum at 700 nm gradually increased when pH decreased from 5.0 to 2.0, which could attribute to protonation of benzimidazole nitrogen (Scheme S1 in Supporting information). Importantly, the protonation of benzimidazole nitrogen makes the emission maxima of SiBM1-3 red-shift to 720 nm due to the enhanced electron-withdraw. After fluorescent pH titration experiments, the pK_a value of SiBM1-3 were calculated as 3.79, 2.79 and 4.28 (Fig. S5 in Supporting information).

Then, we investigated the fluorescence spectra stability of SiBM1-3 in PBS solutions containing H_2O_2, Cys, GSH and $ONOO^-$, which easily quenched the fluorescence of Si-pyronins. As shown in Fig. S6 (Supporting information), SiBMs showed considerable stability toward H_2O_2, Cys, GSH and $ONOO^-$. By using a Xe lamp, we investigated the photostability of SiBM1-3 compared with Cy5.5 under the same conditions. As shown in Fig. 2A, when these dyes were irradiated by the Xe lamp for 15 min, their fluorescence intensity preserved more than 95% and exhibited greater stability than Cy5.5 (70% reserved). All the above data illustrate that SiBM1-3 had good pH stability, chemical stability, and photostability.

Considering the excellent photophysical properties and sufficient stability, we deduced that SiBM1-3 hold great potential for

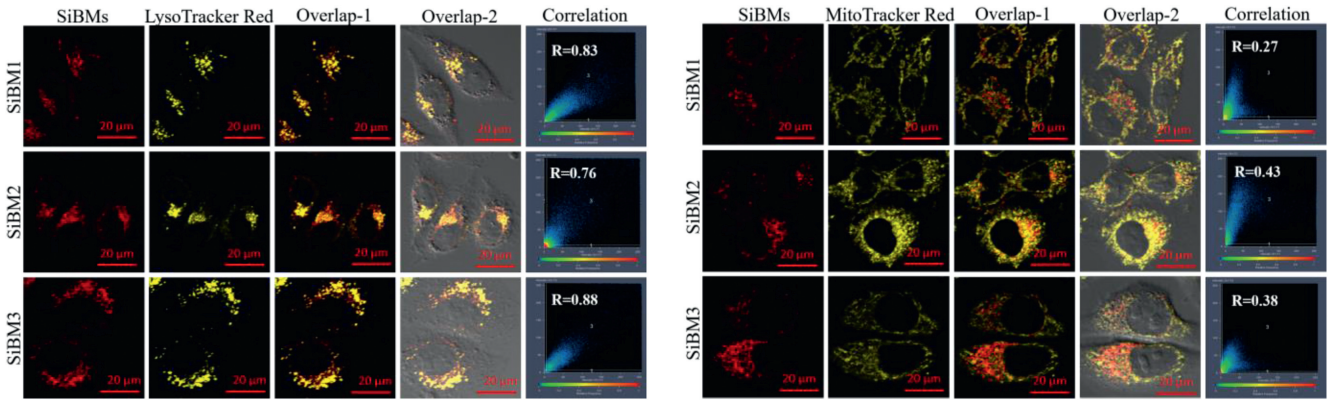

Fig. 3. Confocal images of HeLa cells co-stained with SiBM1-3 (2 μmol/L, 20 min) and LysoTracker Red (0.1 μmol/L, 15 min) in PBS at 37 °C or MitoTracker Red (0.2 μmol/L, 15 min) in PBS at 37 °C. Overlay 1: overlay of the red channel and yellow channel. Overlay 2: overlay of Overlay 1 and bright-field images. For SiBM1-3, the emission was collected at 680–760 nm (λ_{ex}: 633 nm); for LysoTracker Red and MitoTracker Red, the emission was collected at 570–650 nm (λ_{ex}: 561 nm); Scale bar: 20 μm.

imaging in biological applications. Thus, we investigated the cellular imaging performance of SiBM1-3 and tested their cytotoxicity by an MTT assay before imaging in cells. As shown in Fig. 2B, cell viability was above 80% in the case of HeLa cells incubated with SiBM1-3 for 24 h at the range of 1–10 μmol/L, indicating the toxicity was very small. Subsequently, we incubated SiBM1-3 with HeLa cells at 37 °C for 20 min; a bright fluorescence was observed under laser scanning confocal microscopy when excited at 633 nm (Fig. S7 in Supporting information), suggesting that the dye possessed good cell membrane permeability.

In order to determine the subcellular localization, we co-stained SiBM1-3 with commercial LysoTracker Red DND-99 and MitoTracker Red in HeLa cells. As shown in Fig. 3, after co-staining SiBM1-3 with LysoTracker Red DND-99 for 15 min, the yellow fluorescence from LysoTracker and the red fluorescence from SiBMs overlapped well ($R > 0.75$); especially, the Pearson's coefficient of SiBM3 and LysoTracker Red was 0.88 due to the morphine group. By contrast, low Pearson's coefficients were observed when co-staining SiBMs with MitoTracker Red (below 0.45), indicating SiBM1-3 could specifically localize in lysosomes instead of mitochondria. Importantly, the fluorescence intensity of HeLa cells after treating with SiBM1-3 maintained 80% of the original value after continuous irradiation by a semiconductor laser for 10 min. By contrast, under the same conditions, the fluorescence intensity of LysoTracker Red was photobleached below 50% (Fig. S8 in Supporting information), indicating that SiBM1-3 were still photostable in cells.

The superior photophysical properties and outstanding performance in cells encouraged us to expand the application of the SiBMs platform. We synthesized reduced 'dihydro' derivatives (HSiBM1-3) to selectively sense ROS, with reference to dihydrofluorescein (DHF, a widely used fluorescent ROS probe) [34]; its chemical structure was confirmed by ^{1}H NMR, ^{13}C NMR, and HRMS spectra). With HSiBM1-3 in hand, we evaluated their capability to respond to ROS in a PBS buffer solution (20 mmol/L, containing 20% MeCN, pH 7.4), including H_2O_2, ClO^-, $ONOO^-$, $HO^•$, $^1O_2$, $O_2^{•-}$, and NO. As shown in Fig. S9 (Supporting information), HSiBM1-3 were almost non-fluorescent in PBS due to their non-conjugated structure. However, after treating with 5 equiv. of $ONOO^-$, strong fluorescence near 700 nm was observed. More importantly, HSiBM3 had better selectivity toward $ONOO^-$ than HSiBM1 and HSiBM2, which were susceptible to ClO^- and NO. Subsequently, we determined whether HSiBM3 could be photo-oxidized. As shown in Fig. S10 (Supporting information), the fluorescence intensity of HSiBM3 showed almost no change after being continuously excited by a Xe lamp for 10 min, indicating excellent photostability. Therefore, we

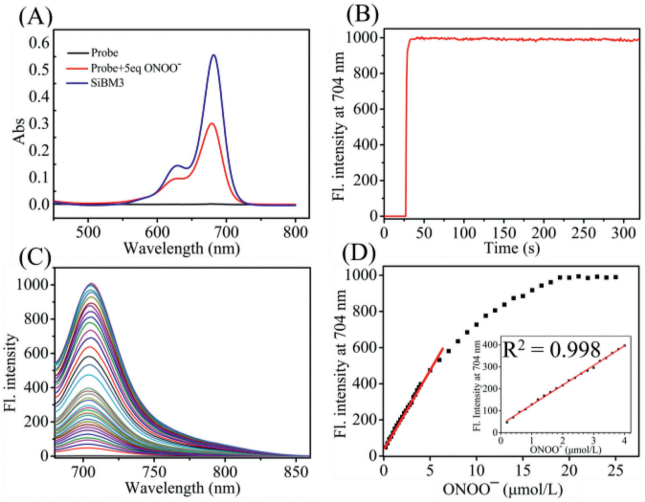

Fig. 4. (A) Absorption spectra of HSiBM3 (5 μmol/L) in PBS (20 mmol/L, containing 20% MeCN, pH 7.4) before and after treating with 5 equiv. of $ONOO^-$ and SiBM3 (5 μmol/L). (B) Time-dependent fluorescence intensity of HSiBM3 (5 μmol/L) treated with 25 μmol/L $ONOO^-$ at 704 nm. (C) Fluorescence spectra of HSiBM3 (5 μmol/L) in PBS (20 mmol/L, containing 20% MeCN, pH 7.4) upon gradual addition of $ONOO^-$ (0–25 μmol/L). (D) Linear correlation between fluorescence intensities of HSiBM3 (2 μmol/L) at 704 nm and concentration of $ONOO^-$. λ_{ex}: 670 nm; $T = 25$ °C.

selected HSiBM3 as an $ONOO^-$ fluorescent probe for further research.

Thus, the reactivity properties of HSiBM3 in PBS (20 mmol/L, containing 20% MeCN, pH 7.4) toward $ONOO^-$ were evaluated. As shown in Fig. 4A, the absorbance of HSiBM3 (5 μmol/L) at 680 nm and its fluorescence at 704 nm were extremely low due to the non-conjugated structure. After reacting with 25 μmol/L $ONOO^-$, an obvious absorption band and strong fluorescence appeared at 680 nm and 704 nm, respectively. The new merged absorption and fluorescence spectral profiles were nearly identical to those of SiBM3, and the HRMS peak at m/z 566.3311 corresponded to SiBM3 (Fig. S11 in Supporting information), revealing that the possible reaction product formed after HSiBM3 was treated with $ONOO^-$ was SiBM3. Moreover, the fluorescence intensity at 704 nm rapidly increased and reached the highest value within 2 s, indicating the extremely fast reaction of HSiBM3 with $ONOO^-$ (Fig. 4B).

Notably, the fluorescence intensity of HSiBM3 (5 μmol/L) at 704 nm also exhibited a fairly linear relationship with the concentration of $ONOO^-$ in the range of 0–4 μmol/L, and the lower limit

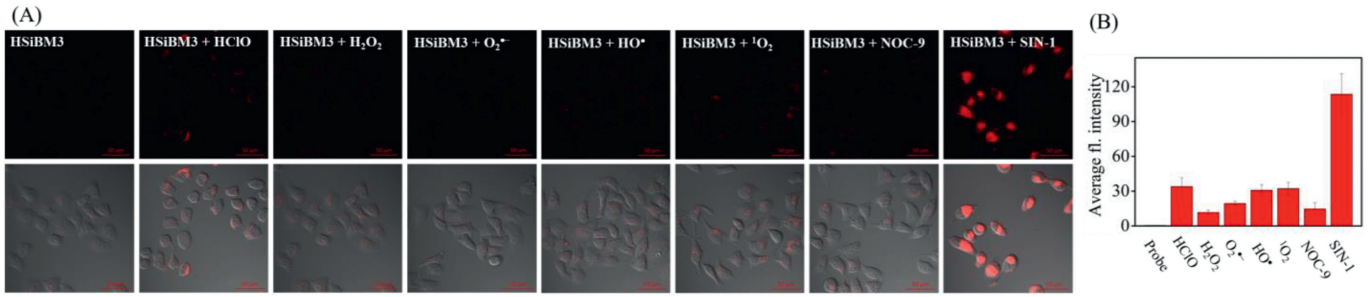

Fig. 5. (A) Fluorescence images and fluorescence-DIC overlay images of HeLa cells pretreated with HSiBM3 (2 μmol/L) for 30 min, and then treated with various ROS in PBS. Including: ClO^- (100 μmol/L), H_2O_2 (100 μmol/L), $O_2^{\bullet-}$ (100 μmol/L), $HO^\bullet$ (Fe^{2+}/H_2O_2: 50 μmol/L/200 μmol/L), $^1O_2$ (ClO^-/H_2O_2: 50 μmol/L/0.5 mmol/L), NO (NOC-9: 100 μmol/L), $ONOO^-$ (SIN-1: 200 μmol/L). (B) Average fluorescence intensity from the imaging results. Emission was collected at 680-760 nm (λ_{ex}: 633 nm). Scale bar: 50 μm.

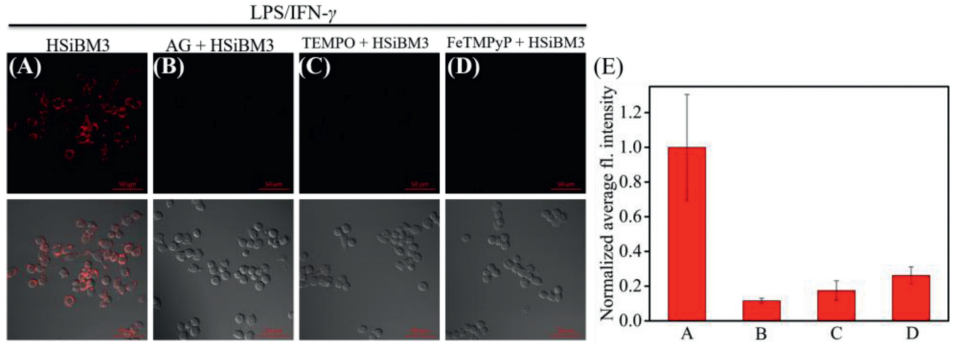

Fig. 6. (A–D) Confocal images of RAW 264.7 cells pretreated with LPS (1 μg/mL)/IFN-γ (50 ng/mL) in the absence and presence of ROS scavengers [AG (0.5 mmol/L), TEMPO (1 mmol/L), and FeTMPyP (200 μmol/L)] for 6 h, at last, treated with HSiBM3 (2 μmol/L) for 30 min. (E) Average fluorescence intensity from images results. Emission was collected at 680–760 nm (λ_{ex}: 633 nm). Scale bar: 50 μm.

of detection (LOD) was determined to be as low as 13.5 nmol/L (Figs. 4C and D). As shown in Fig. S12 (Supporting information), HSiBM3 was non-fluorescent at pH 2-12 and displayed significant fluorescence turn-on responses for $ONOO^-$ at pH 3-8. Taken together, HSiBM3 was shown to be a selective and sensitive fluorescent probe for $ONOO^-$ and thus holds potential for real-time imaging of $ONOO^-$ under physiological pHs.

Before the cell imaging, the cytotoxicity of HSiBM3 in HeLa cells was tested. As shown in Fig. S13 (Supporting information), after incubating under a certain concentration of HSiBM3 (1–10 μmol/L), the cell viability was higher than 80%, indicating a low cytotoxicity and excellent biocompatibility of HSiBM3. Then, we studied the performance of HSiBM3 (2 μmol/L) toward sensing $ONOO^-$ in HeLa cells by laser scanning confocal microscopy. As shown in Fig. 5, the HSiBM3 (2 μmol/L)-loaded HeLa cells were non-fluorescent; after adding various ROS (*i.e.*, H_2O_2, ClO^-, $ONOO^-$, $HO^\bullet$, $^1O_2$, $O_2^{\bullet-}$, and NO), $ONOO^-$ elicited the most obvious fluorescence enhancement when excited at 633 nm, indicating HSiBM3 could selectively image exogenous $ONOO^-$ in the cellular environment. Using the same condition, negligible fluorescence could be observed from HSiBM3 (2 μmol/L)-loaded HeLa cells after being continuously irradiated for 15 min (Fig. S14 in Supporting information), which further illustrated that the fluorescence signal was attributed to the reaction between the HSiBM3 and $ONOO^-$. In addition, we assessed the subcellular localization of HSiBM3 in HeLa cells after treating with SIN-1 ($ONOO^-$ donor). As shown in Fig. S15 (Supporting information), excellent overlapping images between the turn-on single and LysoTracker Red DND-99 were observed, indicating that HSiBM3 localized in lysosomes.

Subsequently, we imaged endogenous $ONOO^-$ in LPS (1 μg/mL)/IFN-γ (50 ng/mL)-treated RAW264.7 cells. As shown in Fig. 6, when the LPS/IFN-γ pretreated RAW264.7 cells were stimulated with HSiBM3 for 30 min, a bright fluorescence was observed. In contrast, extremely weakened red fluorescence was observed when RAW264.7 cells were pretreated with LPS/IFN-γ and ROS scavengers (AG [35], TEMPO [36], and FeTMPyP [37]) for 6 h and then incubated with HSiBM3 for 30 min. Thus, HSiBM3 was a suitable fluorescent probe for imaging $ONOO^-$ in cells, and coupled with being lysosome-targetable, possesses huge potential for studying the relationship between lysosomes and $ONOO^-$.

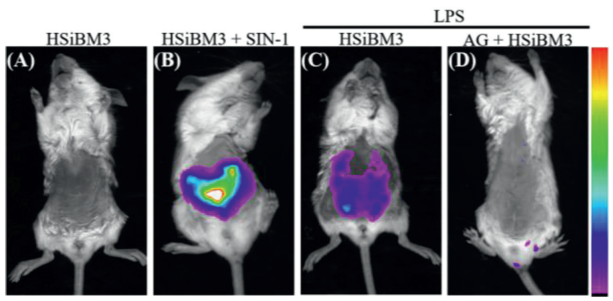

Fig. 7. (A, B) Overlay of fluorescence images and bright field images of mice i.p. injected HSiBM3 (100 μL, 200 μmol/L) in the absence and presence of SIN-1 (100 μL, 500 μmol/L). (C, D) The mouse was first i.p. injected with LPS (1 mg/mL, 100 mL) followed by AG (100 μL, 1 mmol/L) or not for 24 h, and then i.p. injected with HSiBM3 (100 μL, 200 μmol/L). Excitation filter: 630 nm; emission filter: 700 nm.

Given that the emission wavelength of SiBM3 was near the 700 nm wavelength window for deep tissue penetration and minimum background fluorescence, we further investigated the performance of HSiBM3 to image exogenous and endogenous $ONOO^-$ in 8-week-old BALB/c mice. As shown in Fig. 7, almost no fluorescence signal was observed when the mice were intraperitoneally injected with HSiBM3 for 30 min. In contrast, a strong fluorescence signal was observed when the mice were i.p.-injected with HSiBM3

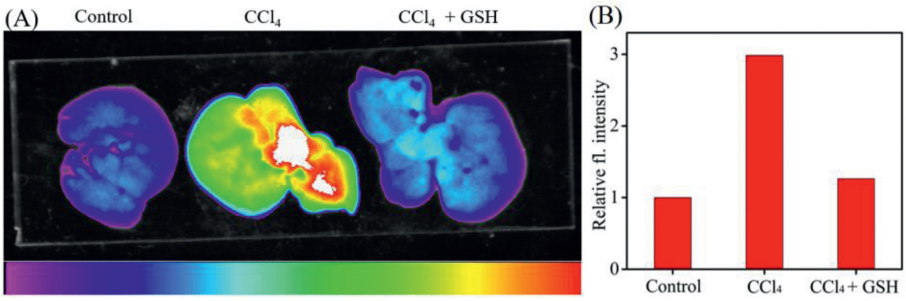

Fig. 8. (A) Fluorescence images of representative livers. Mice i.p.-injected with PBS (as a control) for 24 h, or 20% CCl_4 (10 mL/kg, dissolved in olive oil) for 24 h, or i.p.-injected with CCl_4 and then injected with GSH (150 mg/kg, ROS scavenger) for 24 h, followed by HSiBM3 (100 μL, 200 μmol/L). (B) Relative fluorescence intensity in (A). Excitation filter: 630 nm; emission filter: 700 nm.

and then with the SIN-1 for another 30 min. In addition, when the mice were i.p.-injected with LPS (to induce inflammation) for 6 h, an obvious fluorescence signal was observed after being i.p.-injected with HSiBM3. Almost no fluorescence signal was observed when the mice were i.p.-injected with LPS followed by AG for 6 h before injecting with HSiBM3, indicative of the ability of HSiBM3 to image exogenous and endogenous $ONOO^-$ in living mice.

It was reported that a single intraperitoneal injection of carbon tetrachloride (CCl_4) could induce acute liver injury in mice, and $ONOO^-$ is produced in this process [38]. Thus, we detected endogenous $ONOO^-$ in CCl_4-stimulated mice (to induce liver injury) by HSiBM3. At first, the BALB/C mice were i.p.-injected with PBS (as a control) or 20% CCl_4 (10 mL/kg, dissolved in olive oil) or i.p.-injected with CCl_4 and then injection with GSH (150 mg/kg, ROS scavenger) for 24 h. Then, the mice were injected with HSiBM3 (100 μL, 200 μmol/L) *via* a tail vein for 2 h before isolating the liver for imaging. As shown in Fig. 8, the CCl_4-treated group shows a three-fold fluorescence enhancement compared with the control group. After adding GSH, a remarkable decrease in fluorescence was observed, as compared to the mice only injected with CCl_4. The above results confirmed that HSiBM3 was suitable for *in vivo* detection of both endogenous $ONOO^-$ and hepatotoxicity.

In summary, we have developed three NIR fluorescent dyes (SiBM1-3) by introducing an electron-withdrawing benzimidazole unit at the C9 position of a Si-pyronin dye, which showed an emission wavelength of 700 nm and excellent optical properties. Furthermore, SiBM1-3 showed good cell-membrane permeability and photostability in HeLa cells and could specifically localize in lysosomes. To further exploit the application of the SiBMs platform, we further synthesized reduced 'dihydro' derivatives (HSiBM1-3) and evaluated their sensing performance toward ROS. It was demonstrated that among these probes, HSiBM3 had the best sensing ability for $ONOO^-$, including high selectivity and sensitivity and a fast fluorescence "off–on" response (within 2 s). HSiBM3 was further successfully used for imaging exogenous and endogenous $ONOO^-$ in cells and mice. More importantly, HSiBM3 was successfully employed for visualizing acute-liver-injury-induced peroxynitrite. It is expected that more functional dyes could be developed in the future using this platform.

Ethical compliance

All the animal experiments were carried out in accordance with the relevant laws and guidelines issued by the Ethical Committee of Shanxi University.

Declaration of competing interest

The authors declare that they have no known competing financial interests or personal relationships that could have appeared to influence the work reported in this paper.

Acknowledgments

We acknowledge Scientific and Technological Innovation Program of Colleges and Universities in Shanxi Province (Nos. 2021L529, 2021L530). We also thank Dr. Y.Q. Sun for his assistance.

Supplementary materials

Supplementary material associated with this article can be found, in the online version, at doi:10.1016/j.cclet.2022.06.069.

References

[1] L. Yuan, W.Y. Lin, K.B. Zheng, et al., Chem. Soc. Rev. 42 (2013) 622–661.
[2] H. Kobayashi, M.R. Longmire, M. Ogawa, P.L. Choyke, Chem. Soc. Rev. 40 (2011) 4626–4648.
[3] Z.Q. Guo, S. Park, J. Yoon, I. Shin, Chem. Soc. Rev. 43 (2014) 16–29.
[4] J. Han, X. Yue, J. Wang, et al., Chin. Chem. Lett. 31 (2020) 1508–1510.
[5] X. Ren, L. Liao, Z. Yang, et al., Chin. Chem. Lett. 32 (2021) 1061–1065.
[6] M.Y. Fu, Y. Xiao, X.H. Qian, et al., Chem. Commun. (2008) 1780–1782.
[7] Y. Koide, Y. Urano, K. Hanaoka, T. Terai, T. Nagano, ACS Chem. Biol. 6 (2011) 600–608.
[8] B.G. Wang, X.Y. Chai, W.W. Zhu, et al., Chem. Commun. 50 (2014) 14374–14377.
[9] F. Deng, Z.C. Xu, Chin. Chem. Lett. 30 (2019) 1667–1681.
[10] W. Zhou, X.N. Fang, Q.L. Qiao, et al., Chin. Chem. Lett. 32 (2021) 943–946.
[11] Y. Koide, Y. Urano, K. Hanaoka, et al., J. Am. Chem. Soc. 134 (2012) 5029–5031.
[12] J.B. Grimm, B.P. English, J. Chen, et al., Nat. Methods 12 (2015) 244–250.
[13] M. Li, Y.T. Li, X.J. Wang, et al., Chin. Chem. Lett. 30 (2019) 1682–1688.
[14] M. Du, B.L. Huo, J.M. Liu, et al., J. Mater. Chem. C 6 (2018) 10472–10479.
[15] G.J. Mao, Z.Z. Liang, G.Q. Gao, et al., Anal. Chim. Acta 1092 (2019) 117–125.
[16] J. Wang, D. Cheng, L. Zhu, et al., Chem. Commun. 55 (2019) 10916–10919.
[17] J.F. Miao, Y.Y. Huo, H.P. Shi, et al., J. Phys. Chem. B 6 (2018) 4466–4473.
[18] H.X. Zhang, J. Liu, C.L. Liu, et al., Biomaterials 133 (2017) 60–69.
[19] H.X Zhang, J. Liu, L.F. Wang, et al., Biomaterials 158 (2018) 10–22.
[20] W. Zhu, X. Chai, B. Wang, et al., Chem. Commun. 51 (2015) 9608–9611.
[21] S.N. Uno, M. Kamiya, T. Yoshihara, et al., Nat. Chem. 6 (2014) 681–689.
[22] M.S. Frei, P. Hoess, M. Lampe, et al., Nat. Commun. 10 (2019) 4580.
[23] R. Wirth, P. Gao, G.U. Nienhaus, M. Sunbul, A. Jäschke, J. Am. Chem. Soc. 141 (2019) 7562–7571.
[24] W.J. Liu, J. Chen, Q.L. Qiao, et al., Chin. Chem. Lett. 33 (2022) 4943–4947.
[25] X.L. Li, J.Z. Zheng, W.J. Liu, et al., Chin. Chem. Lett. 31 (2020) 2937–2940.
[26] S. Kaloyanova, Y. Zagranyarski, S. Ritz, et al., J. Am. Chem. Soc. 138 (2016) 2881–2884.
[27] X.Y. Chai, X.Y. Cui, B.G. Wang, et al., Chem. Eur. J. 21 (2015) 16754–16758.
[28] J. Liu, Y.Q. Sun, H.X. Zhang, et al., ACS Appl. Mater. Interfaces 8 (2016) 22953–22962.
[29] T. Pastierik, P. Šebej, J. Medalová, P. Štacko, P. Klán, J. Org. Chem. 79 (2014) 3374–3382.
[30] F. Han, Y.X. Chen, Y.M. Lu, et al., J. Pineal Res. 51 (2011) 124–135.
[31] D.N. Tripathi, R. Chowdhury, L.J. Trudel, et al., Proc. Natl. Acad. Sci. U. S. A. 110 (2013) 2950–2957.
[32] R. Müller, C. Zander, M. Sauer, et al., Chem. Phys. Lett. 262 (1996) 716–722.
[33] Y. Koide, Y. Urano, K. Hanaoka, T. Terai, T. Nagano, ACS Chem. Biol. 6 (2011) 600–608.
[34] S.L. Hempel, G.R. Buettner, Y.Q. O'Malley, et al., Free Radic. Biol. Med. 27 (1999) 146–159.
[35] R.B.R. Muijsers, E. Van Den Worm, G. Folkerts, et al., J. Pharmacol. 130 (2000) 932–936.
[36] P.K. Chatterjee, S. Cuzzocrea, P.A.J. Brown, et al., Kidney Int. 58 (2000) 658–673.
[37] R. Radi, J. Biol. Chem. 288 (2013) 26464–26472.
[38] J.F. Ye, H. Zhu, Z.F. Zhou, Biol. Pharm. Bull. 34 (2011) 1666–1670.